Title

Accurate spatiotemporal retinal responses require a color intensity balance fine-tuned to natural conditions

Authors

Filippo Castellani[1,2,3,*], Awen Louboutin[1,*], Tom Quétu[1,*], Remi Baroux[1], Ulisse Ferrari[1], Matías A. Goldin [1,†]

Affiliations

[1] Sorbonne Université, CNRS, Inserm, Institut de la Vision, F-75012 Paris, France
[2] Politecnico di Milano, Department of Electronics, Information, and Bioengineering, Milan, Italy
[3] Present address: The BioRobotics Institute, Scuola Superiore Sant'Anna, Pisa, Italy

Footnotes

[*] Contributed equally
[†] Corresponding author: matias.goldin@inserm.fr

Summary

Color vision is vital for animal survival, essential for foraging and predator detection. In mice, as in other mammals, color vision originates in the retina, where photoreceptor signals are processed by neural circuits. However, retinal responses to stimuli involving multiple colors are still not well understood. One possible explanation of this knowledge gap is that previous studies have not thoroughly examined how neuronal activity adapts to a 30 seconds to a few minutes timescale when exposed to multiple color sources. To address this, we systematically varied the UV-to-green light balance with a custom-built stimulator targeting mice opsins spectra while recording retinal ganglion cell responses in the ventral retina using multielectrode arrays. Responses to full-field chirp and checkerboard stimulations with alternating UV and green light revealed that more than one order of magnitude of intensity difference favoring green M-opsin over UV S-opsin is needed for a balanced reliability in retinal ganglion cell responses. An incorrect balance, with slightly increased UV light, silenced responses to green illumination. To determine if these values are consistent with natural conditions, we analyzed isomerisation rates in the mouse retina across different times of the day. We found that the M- to S-opsin activation ratio remains constant through the mesopic-photopic range, and our empirically determined values align well with these natural conditions, lying far from a simple equalization of M- and S-opsin isomerisation rates. In conclusion, a finely tuned color intensity balance is essential for accurately measuring both fast temporal responses and detailed spatial receptive fields.

Keywords: retina, retinal ganglion cells, color processing, electrophysiology, light intensity, natural illumination, isomerisation rates

1. Introduction

The number, the type and the distribution of photoreceptors across the retina vary widely among vertebrates, reflecting evolutionary adaptations to their behavior. Radically different configurations can be observed in diurnal and nocturnal animals, as well as depending on their lifestyle, such as whether they are prey or predators (Baden, 2024; Baden, 2020; Peichl, 2005; Peichl et al., 2019; Pessoa et al., 2014; Yoshimatsu, 2020). These adaptations optimize the visual information they can obtain in natural environments, directly influencing their ability to find food, detect predators, and navigate. Color vision, which plays a key role, relies on comparing signals from photoreceptors with different spectral sensitivities determined by their opsins (Osorio et al., 2004; Valenta et al., 2013).

The mouse retina, like in many other mammals but primates (Dacey, 1996; Dacey, 1999), expresses two types of cone opsins, S-Opsin and M-Opsin, with peak sensitivities at 360 nm and 508 nm respectively (Nikonov et al., 2006). Unlike primates, robust cone-opponent cells, crucial for color discrimination, have not been clearly identified in the mouse retina, with the exemption of one intrinsically sensitive ganglion cell (Stabio et al., 2018). In primates, these cells compare input from different types of cones, enabling wavelength discrimination (Field et al., 2010). Some studies suggest that such circuits might coexist in the thalamic region of mice (Mouland et al., 2021), while others propose that certain retinal ganglion cells use rod-cone opponency for color discrimination (Joesch & Meister, 2016; Khani & Gollisch, 2021). Recent studies investigated the origin of color opponency in the ventral retina, tracing it back to interactions at the cone synapse through lateral inhibition from horizontal cells, partially driven by rods (Behrens et al., 2016; Yoshimatsu et al., 2021). Furthermore, bipolar cells relay the chromatic information to retinal ganglion cells, where type-specific, nonlinear center-surround interactions result in color-opponent output channels to the brain (Szatko et al., 2020; Korympidou et al., 2024). Behavioral studies confirm that mice can distinguish between different colors, particularly in the upper visual field, likely due to the distribution of photoreceptors in the retina (Denman et al., 2018).

The expression patterns in the mice retina of the two color opsins create opposing and overlapping gradients along the dorsal-ventral axis (**Fig. 1a**) (Szel et al., 1992). As a result, the majority of cones express both opsins. However, there are also cones that exclusively express one opsin. Thus, S-Opsin enrichment in the ventral retina may help the detection of short-wavelength light from the sky, and M-opsin in the dorsal retina permits the perception of the ground (e.g., a grassy field), while co-expression of both opsins broadens the spectral range of individual cones and improves perception under varying conditions of ambient light. A recent study suggested that the nonlinear interaction of UV and green would serve to delineate the threshold between the sky and the ground (Khani & Gollisch, 2021). The ventral portion of the mice retina emerges as an ideal system for investigating color processing capabilities (**Fig. 1b**). Moreover, although the role of rods in color discrimination is not fully understood, there is a close overlap in spectral sensitivity with the M-opsin (Wang et al., 2011; Govardovskii et al., 2000). Their influence on the overall retinal response is significant, particularly in their potential contribution to green color detection at high illumination levels (photopic regime) (Adelson, 1982; Khani & Gollisch, 2021; Tikidji-Hamburyan et al., 2017; Pearson et al., 2015).

Understanding retinal visual processing has long relied on simplified, artificial stimuli, which have been instrumental in uncovering key properties of the retina (center-surround antagonism, non-linear spatial integration, contrast computation, etc.). However, recent studies using natural images and videos (Höfling et al., 2024; Franke et al., 2022) emphasize the importance of natural scene statistics (Tkačik et al, 2011; Atick et al., 1992; Doi et al., 2003) in revealing complex nonlinear processes within the retinal circuit (Goldin et al., 2022; Goldin et al., 2023; Goethals et al., 2024; Karamanlis et al., 2022; Turner et al., 2018; McIntosh et al., 2016; Maheswaranathan et al., 2023). While artificial stimuli remain valuable for probing specific retinal functions, they do not fully capture how the retina operates in real-world conditions, making natural stimulation a fundamental tool. The incorporation of color into these stimuli can significantly enhance our knowledge of retinal circuits (Khani & Gollisch, 2021; Hofling et al., 2024; Qiu et al., 2021; Szatko et al., 2020; Fornetto et al., 2024). However, despite technological advancements that allow for precise measurement of color information in natural scenes (Franke et al., 2019; Qiu et al., 2021), there are still limitations on the length of experiments where these stimuli can be presented in vitro. This poses challenges, especially when investigating the nonlinear interactions that occur when multiple colors are present.

Natural scenarios can have different color content, such as with night or light day illumination. Therefore, depending on the animal adaptation to its environment, the proper balance between the intensities of the chromatic information present in a natural stimulation can have different impacts on the nonlinear processing of visual information by the retinal circuit. In addition, light entering the eye can be differentially absorbed by the optics media of the eye depending on the wavelength of the incident light, thus modifying the chromatic content of natural scenes arriving at the retina (Henrikson et al., 2010; Douglas & Jeffery, 2014). Shorter wavelengths will be less transmitted, thus having less intensity at the photoreceptor layer of the retina at the back of the eye. Thus, in order to approach a more naturalistic stimulus design, natural illumination levels should be taken into account.

Studying color processing in the ex-vivo retina can also be impacted by the recording technology chosen. Considerable light activation of the photoreceptors can occur when using functional imaging to record retinal activity. Single or 2-photon microscopy aimed at activating different types of indicators, such as Calcium or glutamate indicators, can put the retina in a high mesopic/low photopic light regime (Euler, Franke & Baden, 2019). The chromatic content of the activation light is not flat in the light spectrum but is considerably higher where the M-opsin presents its higher absorption. This issue has been recognized and it was considered to just reduce the contrast of the stimulation provided to the retina. But, can the unbalance in the color content of this background stimulation have other effects on retinal processing?

Our study here thus aims to determine the effect of changing the ratio of S-opsin to M-opsin isomerisation rates on retinal responses when using color stimuli. Our goal is to identify the UV and green light intensities that best allow us to study retinal computations involving both colors in mice. To guide our search, we will assess the reliability of the responses of ganglion cells for different color configurations and quantify their responses to fast temporal and fine spatial features that we will test using a chirp and checkerboard stimuli respectively. In the following sections, we will first detail our methods, including the

experimental setup and the versatile color stimulation tool we developed, along with the selected stimuli used to test retinal responses. We will then present our results, highlighting the best balance S-, M-opsin isomerisation rates ratio for studying color processing in the retinal circuit. We will finally compare our empirically found ratio to the ones found in a natural setting at different times of the day. Finally, we will discuss the implications of our findings.

2. Methods

2.1 Electrophysiological recordings

Electrophysiological data were obtained from isolated retinas of six C57BL6J mice, aged 7 to 17 weeks. The experiments adhered to the institutional animal care standards of Sorbonne Université. After euthanizing the animal, the eye was enucleated and swiftly transferred to oxygenated RINGER medium (for 2L: NaCl 125 mmol/L (14.61 g), KCl 2.5 mmol/L (0.373 g), $MgCl_2 \cdot 6H_2O$ 1 mmol/L (0.407 g), $NaHCO_3$ 26 mmol/L (4.369 g), $CaCl_2$ 1 mmol/L (0.294 g), L-glutamine 0.43 mmol/L (0.126 g), NaH_2PO_4 1.25 mmol/L (0.300 g), Glucose 20 mmol/L (7.206 g)). Dissection was carried out under dim red light. A ventral section of the retina was mounted onto a transparent dialysis membrane and positioned with the ganglion cell side facing a 252-channel multi-electrode array (MEA) with electrodes of 8µm of diameter and spaced 30 µm apart. Throughout dissection and recording, the tissue was perfused with oxygenated RINGER solution using a peristaltic perfusion system with two independent pumps: PPS2 (Multichannel Systems GmbH). Retinas were maintained at 36 degrees during the entire experiment.

Data was sampled at 20 kHz. The raw signals were high-pass filtered at 100 Hz, and spikes were detected using SpyKING CIRCUS (Yger et al., 2018). Subsequent analysis was performed using custom Python scripts. We extracted the activity of 1037 neurons, retaining only those cells with a low number of refractory period violations (< 0.5%, with a median at 0.041% across all experiments, 2 ms refractory period) and well-distinguished template waveforms. These criteria ensured the high quality of the reconstructed spike trains.

2.2 Color stimulation

Two LEDs (Thorlabs Inc.) with peak wavelengths of 385 nm and 530 nm were used as light sources (**Fig. 1c**). Their intensity was adjusted via a microcontroller (Arduino Uno) connected to a multi-channel 12-bit Digital-to-Analog Converter (Module PmodDA4, DILIGENT). The output from the converter was routed to a custom-built constant voltage multiplier for each LED, allowing an output range of 0-5V. Through SPI communication with a computer, we varied the analog voltage values on individual channels. These values were input to a voltage-to-light intensity controller (Thorlabs Inc.) with a maximum frequency of 1 kHz. The light beams from the LEDs were combined into a single multicolor beam using dichroic mirrors and then directed through an optical fiber to a Digital Mirror Device (DLP9500, Texas Instruments). The pixel size obtained at the retina is 3.5 µm. This color stimulation tool has the capability of changing light intensity value and color at a high frame rate. The combined

light was focused on the photoreceptors using standard optics and an inverted microscope (Nikon). The schematic of the setup is shown in **Fig. 1d**.

2.3 Light intensity measurements

We measured the light intensity curves $P(\lambda)$ of the LEDs, where λ denotes the wavelength, using a high resolution spectrometer (USB 200+, Ocean Optics). The total power across the LED spectrum was measured with higher absolute sensitivity using a power meter compact photodiode (PM100D, Thorlabs). Neutral density reflective filters of 15 OD (Thorlabs) were used to decrease the power of the LEDs during the experiments, in order to remain in the central dynamic range of the LED voltage controller when changing the intensity by several orders of magnitude.

2.4 Isomerisation rates calculation

The continuous theoretical form to compute the photoisomerisation rate N ([isomerisation events/(photoreceptor . second], which we will note from now on [iso/ph.s]), given an emission spectrum $P(\lambda)$ in [photons/sec·µm²·nm] is expressed as (Breuninger et al., 2011):

$$N = \int P(\lambda)\, a_C\, S_{abs}(\lambda)\, d\lambda \quad \text{(Eq. 1)}$$

in discrete terms, this formula becomes:

$$N = \sum P(\lambda)\, a_C\, S_{abs}(\lambda)\, \Delta\lambda \quad \text{(Eq. 2)}$$

where $P(\lambda)$ is the stimulation light spectrum, S_{abs} is the normalized absorption spectrum for the photoreceptor's opsin with an amplitude equal to 1 at the peak wavelength and a_C is the "effective light collecting area" of the opsin measured in µm². This effective light collecting area takes into account several factors affecting the probability of photon absorption by opsins: quantum efficiency, which depends on the wavelength, the concentration and availability of opsins (i.e., transmembrane proteins not already engaged in the photoisomerisation cycle) and geometric factors of the photoreceptor. For mice, a_C has been experimentally determined to be 0.2 µm² for cones (Breuninger et al., 2011) and 0.5 µm² for rods (Nikonov et al., 2006).

The absorption spectrum S_{abs} is specific to each opsin and can be sourced from existing literature for cones (**Fig 1c**, Stockman & Sharpe, 2000). For the rhodopsin curve we used the curve from (Rieke-Lab_/calibration-resources github repository), whose short wavelength spectrum lies in between the curve from (Stockman & Sharpe, 2000) and the universal template from (Govardovskii et al., 2000). The remaining values needed to compute isomerisation rates come from the light spectra of each LED $P_1(\lambda)$, $P_2(\lambda)$. We measured them after they have traversed the transparent MEA, to account for reflections and optical

losses. This is important if the lenses used for the light imaging path are coated for the visible spectrum with a cutoff around 400 nm. These light spectra were discretized with a step size of $\Delta\lambda$=0.5 nm.

With this data we could calculate the isomerisation rate for each photoreceptor's opsin by summing the effect of each LED: $P(\lambda) = P_1(\lambda) + P_2(\lambda)$. By adjusting the intensity of each LED, different balance between the two LED spectra can be created using the following formula: $P(\lambda) = a_1 P_1(\lambda) + a_2 P_2(\lambda)$, where a_1, a_2 are values between 0 and 1 representing the normalized modulation of the LED maximum driving voltage to achieve the desired light combination.

In the following of the article, we will use S* , M* or R* to refer to the N isomerisations/photoreceptor.seconds in S- and M- opsins, and rhodopsin respectively, resulting from the maximum illumination intensity selected for each stimulus.

<u>Cross-opsin activation with LED light illumination:</u> Our light sources also activate rhodopsin. From the close overlap we see in **Fig. 1c** between M-opsin and rhodopsin, their isomerisation rates M* and R* are similar. When our green light is turned on, the ratio between M* and R* is: R*/M*=2. Since we cannot activate rhodopsin or M-opsin independently, we will report only the M* value, since we know that R* will vary accordingly. We cannot rule out that the effects on the responses of ganglion cells can be modulated by the rod pathway, but since we will work on the high-mesopic / photopic level, we expect that the contribution to green color responses will be mostly due to M-opsin activation. The isomerisation rate ratio between M* and S* due to our green light is negligible (S*/M*=1.3x10^{-6}). We will report in what follows only the value of M* for the green illumination.

Another unavoidable cross-activation appears when using our UV light, since the tail of the absorption curves of M-opsin and rhodopsin extend well into the short-wavelength side of the spectrum (**Fig. 1c**). When our UV light is turned on, the ratio between M* and S* is S*/M*=4.3, and between R* and S* is S*/R* = 1.2. Although there is less than one order of magnitude difference between of S* and M*, they will be very small compared to the values we will elicit with the green light used in our experiments. In what follows, we will only report only the value of S* for the UV light.

2.5 Checkerboard stimuli

We displayed a random binary checkerboard at 30 Hz to map the receptive fields (RFs) of ganglion cells, consisting of 40 x 40 checks with a check size of 52.5 µm. This size was chosen to have high spatial resolution in the RFs of neurons, in relation to their average size which is above 100 µm. The stimuli contained 20 s long repeated sequences interleaved with 20 s long unrepeated ones. The former are used to test for recording stability, and to quantify reliability in ganglion cell responses. We also use them to calculate firing rates and color onset responses, while the latter unrepeated sequences are used to retrieve the RFs of ganglion cells by calculating a Spike Triggered Average (STA) from their responses. The checkerboard lasted 30 min for a single color and 1h for interleaved two-color recordings.

Building STAs: A three dimensional STA (x, y and time) was sampled using 21 time samples. The spatial STA we display in the figures is obtained as the 2 dimensional spatial slice at the maximum value. To display the STAs we zoomed in a 20 x 20 checkerboard (1,05 mm x 1,05 mm) centered on the RF of each cell.

Fitting RFs: To visualize the RF of each cell with the STA response, we first do a local smoothing of the spatial STA:

$$p_i = 0.8\, p_i + \sum_j 0.2\, p_j \quad \text{(Eq. 3)}$$

where p_i is any RF pixel coordinate and p_j refer to the eight neighbor pixels.

Second, we do a normalization so that $max|STA| = 1$, and do a thresholding to denoise the background by putting to 0 all absolute values below 0.2. To denoise the signal, we do a second smoothing consisting of an exponential sharpening of the STA with a 1.25 exponent with sign preservation: $sign(STA) \cdot exp(log(|STA| \cdot 1.25))$. The value 1.25 was the lowest that we could find that provided a good fit on the following step. Third, we fit a 2-dimensional Gaussian on the resulting spatial STA. The ellipse corresponding to a contour of 20% from the maximum of the fit is used to delineate the spatial RF. This RF is plotted on top of each spatial STA, when it is detected.

Detecting RFs: We evaluated the presence or absence of each cell's STA at different light levels with a 'detection' procedure. We used the RF ellipse contour obtained from the fitting described above and the spatial STA, without smoothing and denoising, and applied the following procedure: first, we check that the center of the fitted ellipse falls sufficiently close to the MEA electrodes position (the central 36% of the full checkerboard area), so that the neuron recorded may have likely received a stimulus input from where the ellipse is located. Second, we calculate the RF area from which we extract an effective radius, as if it was a perfect circle: $r = \sqrt{A/\pi}$. We restrict this radius to lie within 100 and 500 µm as reported in (Baden et al., 2016). Third, we calculate a signal to noise ratio $SNR = \frac{in}{out}$, where *in* is the absolute sum of all the STA values inside the RF, and *out* is the sum of the absolute averaged outside of the RF values. Each averaged outside value is obtained by averaging each line of the spatial STA outside of the RF. An arbitrary threshold of 2.75 is applied on this metric which we found was reasonable at detecting an STA. Then, a cell has a detectable STA if it fulfills the three conditions above.

Quantifying firing rates: To measure firing rates during the repeated checkerboard sequences, we count the number of spikes in two time windows to separate the transient from the sustained responses. The transient range is 0-2 s and sustained range is 2-20s after a color change in the stimulus. This count is then divided by the number of seconds and the number of repeats to obtain a firing rate in Hz. We used this measure to also quantify the firing rates of the chirp stimulus described below.

Quantifying Reliability: To quantify the reliability of ganglion cells responses across repetitions, the average inter-trial correlation was calculated. We considered a 2-20s range from the checkerboard: the unrepeated part of the checkerboard spanned a 20-40 s range, and the 0-2s had a strong transient response due mostly to the previous UV illumination.

Therefore, we computed a 2-20s response histogram (bins of 40ms) for each cell and trial, and we calculated the correlation between these histograms, across all possible pairs. The reliability of a cell in response to the checkerboard stimulus is defined as the average of these correlation values. We used this measure to also quantify the reliability of the chirp stimulus described below.

Quantifying Recovery: To quantify the recovery during the checkerboard responses, the reliability and the RF detection were calculated on an only green illuminated checkerboard (1 x 10^4 M*) presented right after the interleaved two-color illuminated checkerboard (1 x 10^4 M* and 1 x10^4 S*). This checkerboard was divided in two ways: 1) using 6 consecutive windows of 440 s; 2) using a 1800 s sliding window with a 320 s step size. On these windows, the reliability calculation and RF detection were applied. The ganglion cells were divided into two groups comparing their behavior between M*/S*=20 and M*/S*=1, cells that lost a green RF and cells that maintained a detectable green RF. The values calculated during the green checkerboard during the interleaved two-color stimulus were used as the baseline from which the subsequent recovery was compared.

Calculating Recovery time: To calculate the time to reach a steady-state firing rate during the repeated green interleaved checkerboard, we fitted a sigmoid with this formula: $s(x) = a/(1 + e^{c(x-b)})$ to the 2-40s firing rate histogram (thus ignoring the transient 0-2 s peak). The τ, time to return to steady state, was calculated as the time the sigmoid reached 75% of the steady-state value.

2.6 Chirp stimuli

We applied a full field 'chirp' stimulus composed of ON and OFF steps, plus varying frequencies and amplitudes, with luminance values ranging from 0 to 1 (Baden et al., 2016). It was played at 50Hz, containing 20 repetitions of 32 s length each. In the case of the multicolor illuminated chirps we interleaved them, alternating 32 s of UV and 32 s of green illumination.

Quantifying firing rates and reliability: The same methods were used to quantify the firing rates and reliability of the chirp. These measures were calculated on two parts of the chirp, responses to the steps (0-7s) and responses to the fast modulation (9-27s).

2.7 Acclimatation stimulus

Before each protocol, we present a green (530 nm) color illuminated checkerboard to acclimate the retina. These acclimatations were done to ensure a reliable response of the retina to our protocol, while waiting also for a proper stabilization of signals and temperature after the retina was placed on the MEA.

For the green/violet checkerboard stimuli (Fig 2), a green checkerboard at 1 × 10^4 M* was presented for 40 to 45 minutes. For the chirp stimulus (Fig 4), we presented a checkerboard at 1 × 10^4 M* for 44 minutes.

2.8 Statistical tests

To compare the differences between the ganglion cell responses to the two interleaved colors, a paired Wilcoxon signed-rank test was used to find when the difference in responses reverted across conditions. This test was used for the reliability and firing rates of the two-color illuminated checkerboards and chirps (Fig. 2, 4). To test for the recovery of reliability of green checkerboards after presentation of a 1 x 10^4 S* violet illumination, a paired Wilcoxon signed-rank test was used to test if the reliability increased for each step (Fig. 3a, 3b). Finally to test the impact of the cell polarity on firing rates, reliability and firing rates ratios, we used a Wilcoxon-Mann-Whitney test.

2.9 Daylight spectral intensity curves

Single wavelength light: We approximated a light of a single wavelength with a delta function: $P(\lambda) = A\, e^{-(\lambda-L)^2/\sigma^2}$, where A is the amplitude, L is the peak wavelength, λ is the wavelength, and $\sigma = 0.01\ nm$ is the width we used. We searched for the L values that elicited M*/S* ratios between 10 and 60.

Daylight spectra: Data from Yu et al., 2023 was used as natural daylight illumination. The curves were extended to the low wavelengths obtaining the missing range data from Allen et al., 2014. To incorporate the low range with the correct continuity to the different daytime curves consisted of normalizing the low range data, multiplying it by the lowest irradiance value of the curve we wanted to extend, and then incorporating this missing range. Then, to realistically calculate the isomerisation rate produced by these natural light spectra in the retina of mice, we multiplied them by the transmittance of the full eye of the mouse (Henrikson et al., 2010). The obtained $P_{nat}(\lambda)$, natural light spectra curves, are then used in equation 2 to obtain S* and M*.

3. Results

We will start by showing the disappearance of receptive fields (RFs) from checkerboards with green illumination (from now on green checkerboards), and the absence of high frequency responses from green illuminated chirps (from now on green chirps) when we interleave checkerboards or chirps with UV illumination (from now on interleaved UV-green checkerboards or interleaved UV-green chirps) that have S* in the near photopic range. We will then present the procedure with which we found a color balanced S* to M* ratio so that the reliability of the responses across repetitions, and the number of RFs detected under both UV or green checkerboard are the same. We will show that this effect is reversible in the order of a couple of minutes and that it does not depend on single cell firing rates. In a second phase, we will show that the S*-M* balance is similar for a full field chirp stimulation. We will end up by estimating the S*-M* ratio elicited in the retina of mice in natural environments and propose a range of illumination ratios suited to study ganglion cells such that they present reliable responses. We will also quantify ideal narrowband and typical commercial LEDs to see which can stimulate mice photoreceptors within this range.

3.1 Equal S* and M* levels prevent ganglion cell responses to green illumination

We measured RFs in the retina of the mouse in the photopic range using our interleaved UV-green checkerboards (see 2.5). Our chosen level of M* was similar to the one used in many experiments using broadband light stimulation in the high mesopic/near photopic level, whether using a single white LED or a simultaneous combination of UV and green sources (e.g. Goldin et al., 2022; Baden et al., 2016, among many others). Similar isomerisation rates are used during optical measurement of retinal activity when using indicators for intracellular Ca^{2+} levels, i.e. calcium imaging, as a proxy to the spiking activity of ganglion cells (Franke et al., 2019; Höfling et al., 2024; Korympidou et al., 2024). We could not find any reference recommending the use of a reasonable ratio between M* and S*, therefore, to start with, we made the S* level to be identical to M*, as it is the approximate ratio used in many studies (Rosa et al., 2016; Stabio et al., 2018; Szatko et al., 2020). One study used a mix of green and UV light with a M*/S*= 30 to determine the location and size of RFs. By varying independently UV and green they extracted the RFs contributions from the M and S opsins (Joesch & Meister, 2016). In our work, the S* and M* values were then both set at 1 x 10^4 iso/ph.s. In many of the ganglion cells we recorded, the RFs produced by the green checkerboard could not be detected (60% of cells), while the ones produced by the UV checkerboard were present in 82% of the cells (**Fig. 1e**).

Our initial attempt to equalize the activation for S- and M-opsin was inadequate to retrieve both UV and green illumination induced RFs during interleaved UV-green checkerboards. We sought then to study whether a similar effect was present during full field color light stimulation. For this, we stimulated the retina using interleaved UV-green chirps (see 2.6). The responses to the step part of the chirp were not abolished (**Fig. 1f**, 0-12 s range), but the fine temporal structure of the ganglion cell response to high frequency and amplitude fluctuations vanished (**Fig 1f**, 12-32 s range) for most of the cells (47%). We can see that the light step responses at the beginning of the chirp for this example ON cell are still present and slightly diminished compared to the responses to UV, but however the response to the fast varying part of the chirp is absent.

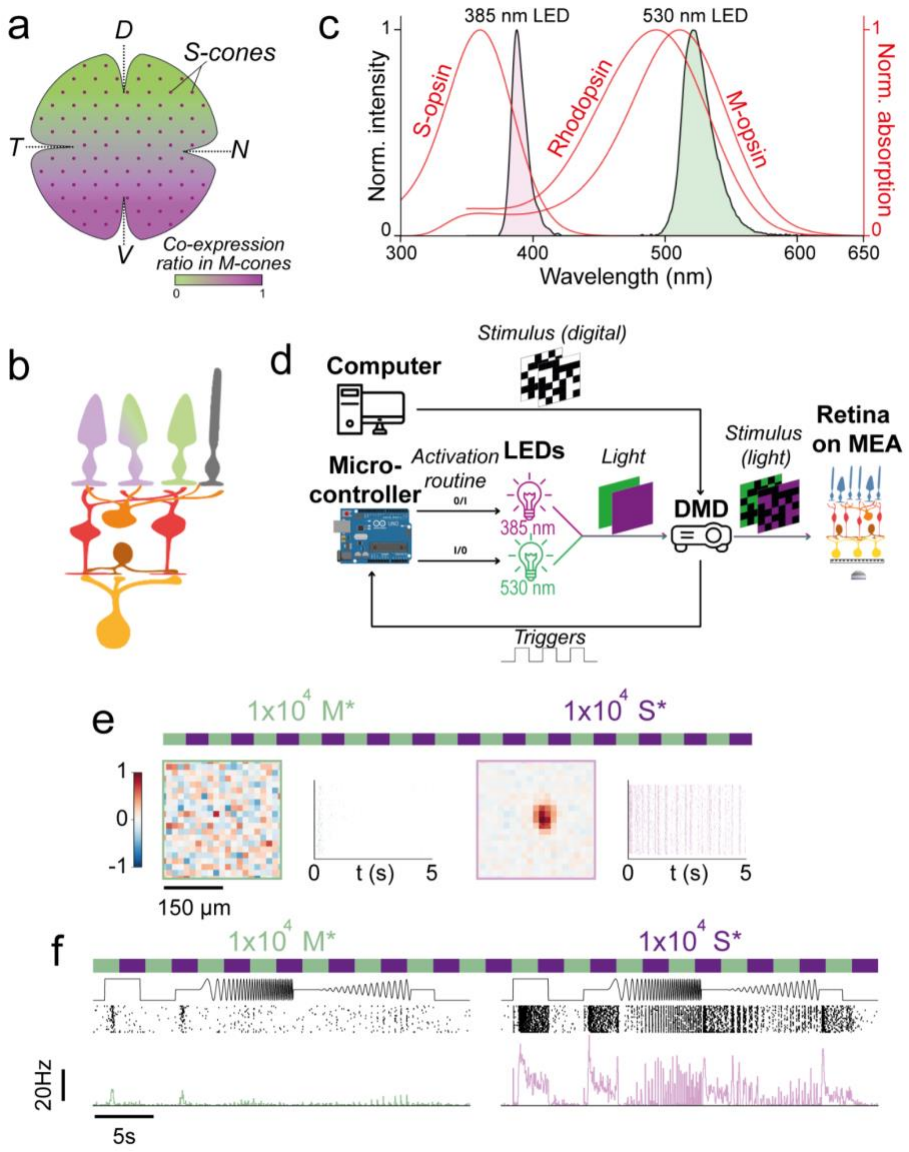

Figure 1 | Interleaved identical activation of S- and M-opsin prevents high resolution and high frequency ganglion cells' responses to green light. a. Schematic distribution of cone photoreceptors across the mouse retina. Dots represent distribution of true S-cones and shading co-expression ratio of S- and M-opsin in M-cone. d: dorsal, n: nasal, v: ventral, t: temporal. **b.** Schematic of the information pathways from photoreceptors to a ganglion cell. Top: Green (M-Opsin), UV (S-Opsin), Green+UV (M-S-opsin co-expression) and Gray (rod). Information is relayed to and processed by middle layer cells (horizontal, bipolar and amacrine) before reaching a ganglion cell (bottom). **c.** The normalized absorption spectra of S-Opsin, M-Opsin and rhodopsin overlaid with the normalized power spectra of UV (385 nm) and green (530 nm) LEDs. The opsins have overlapping absorption spectra, with M-Opsin and rhodopsin extending into shorter wavelengths. This overlap makes it impossible to stimulate S-Opsin without also affecting M-Opsin with the 385 nm LED, though the effect is small. **d.** Schematic of the experimental setup for Multi-Electrode Array (MEA) recordings with a color stimulation device. Two LEDs (385 nm and 530 nm) are modulated via a microcontroller, combined into a single beam using dichroic mirrors, and transmitted through an optical fiber to a Digital Mirror Device (DMD). The light is then focused onto the retina, positioned with the ganglion cell layer in contact with the MEA electrodes, on the back focal plane of a microscope. **e**. Example cell STA and spike raster responses to an interleaved green (left) and UV (right) checkerboard (40s bouts). The response to green is altered. Scale bar: from dark (blue) to bright (red). **f.** Example cell PSTH and spike raster response to an interleaved green (left) and UV (right) chirp (32s bouts). The response to green is altered. The horizontal green and violet bars represent the alternated color stimulus.

3.2 An S*-M* ratio for reliable color responses to interleaved UV-green checkerboards

In pursuit of nonlinear summation of green and UV flashed full field illumination, a study (Kani and Gollisch, 2021) found multiple UV-green contrast balance points for different cells. Other works focused on color opponency using full field or they stimulated the center/surround of the cell's RFs with different spectral content (Szatko et al., 2020; Korympindou et al., 2024). These studies evaluated the strength of the responses during the first hundreds of milliseconds after the ON or OFF illumination steps. On the contrary, here we want to determine the effect of interleaving green and UV at a 30-40 s timescale. We will look for a ratio of M* to S* that provides similarly strong and reliable responses for both UV and green checkerboards. This will in principle allow us to retrieve one UV RF and one green RF per cell, enabling the study of color response structure in a finer scale. While this configuration may not match the exact color balance present in natural conditions, it may be essential for studying more detailed spatial integration properties of the retinal circuit during color stimulation, and as we will see below it falls very close to it.

To find the M* to S* ratio that balances the reliability of responses to UV and green light, we first verified that an only green illumination with M*= 1 x 10^4 iso/ph.s allowed us to retrieve green RFs (example in **Fig. 2a**, top, left, during acclimatation checkerboard). We then used in the same retina a low value of S*= 5 x 10^1 iso/ph.s and found we could retrieve UV RFs in some ganglion cells (example in **Fig 2a**, top right). With these stimuli we were able to detect RFs in 34% and 27% of cells for green and UV checkerboard respectively (see 2.5). The low value for green checkerboard is because it was obtained during the acclimatation checkerboard; the low amount of detected RFs for UV is because the S* used did not elicit a reliable firing rate in the cells. We then stimulated the retina with interleaved UV-green checkerboards, keeping the value of M* constant and increasing the value of S* from 5 x 10^1 to 1 x 10^4 iso/ph.s. When we interleaved UV and green checkerboard with the lowest S* (using the M* and S* we tested above for green and UV only checkerboard), we lost 78% of UV RFs, detecting them in only 6% of the cells (**Fig. 2a**, second row). The firing rate in response to the UV portion was also affected, in comparison to when we used a UV only checkerboard (**Fig. 2a**, first vs second row). When increasing S*, both the reliability and the firing rate of the ganglion cells in response to UV checkerboards increased (**Fig 2a**, UV raster plots, see 2.5). In this manner, we found a M*/S* ratio where we detected a similar number of UV RFs and green RFs (N=217 cells, 72% for UV 67% for green, **Fig. 2a**, bottom), and whose reliability in the response to the repeated sequences was similar (0.09$\pm$0.09 vs 0.14$\pm$0.12 for UV vs green average population responses). The balanced configuration we found was for M*= 1 x 10^4 iso/ph.s and S*= 5 x 10^2 iso/ph.s, resulting in a ratio of M*/S*= 20 (reliability 0.29 for green and 0.17 for violet, for cell in **Fig. 2a**).

We then continued to increase the S* until it reached the same value as M* (example cell in **Fig. 2b**). We retrieved the same effect described in the section above: a strong decrease in the detection of RFs obtained with the green checkerboards. We also saw that the reliability and the firing rate of the ganglion cells in response to the repeated green checkerboard diminished strongly (**Fig. 2b**, green raster plots). However, in contrast to the UV raster plot responses when UV RF were undetectable (**Fig. 2a**, top right), there remained a strong transient response to the onset of the green checkerboard. This can explain why this configuration, which strongly suppresses green responses, is generally used in the

literature to study color responses in ganglion cells: if we restrict ourselves to the first hundreds of milliseconds after a green illumination onset, we can measure a strong firing rate response.

We wondered next if the effects we found were reversible, and presented again the initial green only checkerboard in the same retina. We found that the green RFs came back to the same detected proportion as in our balance configuration (68%, example cell in **Fig. 2c**). To determine a balanced M*/S* ratio, we tested whether the reliability was higher in response to UV checkerboards than to green ones for the paired illuminations tested (**Fig. 2d**). We found that the reliability of UV responses surpassed the green ones at the ratio of M*/S*= 1 (S*= M*= 1 x 10^4 iso/ph.s), while it was the opposite when M*/S*=20. Thus a balanced reliability likely lies between these two values. When we looked for the balance ratio in terms of RFs detectability, we saw that the value of M*/S*= 1 had a very similar number of RFs for each color stimulation, with a slightly higher number for UV (**Fig. 2e**), meaning that a balance configuration would have appeared with a higher M*/S* ratio (lower S* for our fixed M*). We then studied the firing rate responses to the green checkerboard, separating them into a sustained (2-18 s, **Fig. 2f**) and a transient (0-2 s, **Fig. 2g**) response. We found that for the sustained response, the balance ratio was achieved in the same range as the one we found studying the reliability. However, for the transient response the balance was achieved at our tested value of M*/S*=20 (paired two sided Wilcoxon test p*>0.6).

Regarding the undetectability of the RFs at the ratio M*/S*=1, we studied their evolution starting from the balance configuration at M*/S*=20. All the cells that had only a green RF kept it at the higher S* tested, thus the ones that lost their green RF were found only among the cells having both RFs (52% of the cells). From these cells, 31% lost their green RF, 3% lost their violet RF, 3% lost both, and 61% did not show a change (**Fig. 2h**). This result indicates that for a cross-color effect to be present in the ganglion cells, i.e. UV affecting the color response to green, they have to be sensitive to the information coming both from UV and green.

We then studied the temporal properties of the STAs, to find if there was a noticeable contribution to ganglion cell responses from rhodopsin, through R*. We saw that the green temporal STAs obtained at M*/S*=20 were only slightly slower than the UV temporal STAs (t-test p*<0.01, **Fig. 2i,** left). The difference in latency between both on average was 50ms. This was much faster than the peak responses reported from rhodopsin activation (Joesch & Meister, 2016; Nikonov et al., 2006). It has also been shown that rod-mediated responses are bleached by exposing the tissue to a green LED stimulus delivering R*=1.6x10^6 iso/ph.s for 2 minutes, and that there is no recovery following the bleach, even after up to 1 hour of measurement (Wang & Demb, 2011; Wang & Kefalov, 2009). So we applied increasing M* levels and measured the green temporal STAs, without significant changes in their latency (**Fig. 2i**, right), thus showing that most of the responses to the green checkerboard we measured came mainly from M-opsin activation.

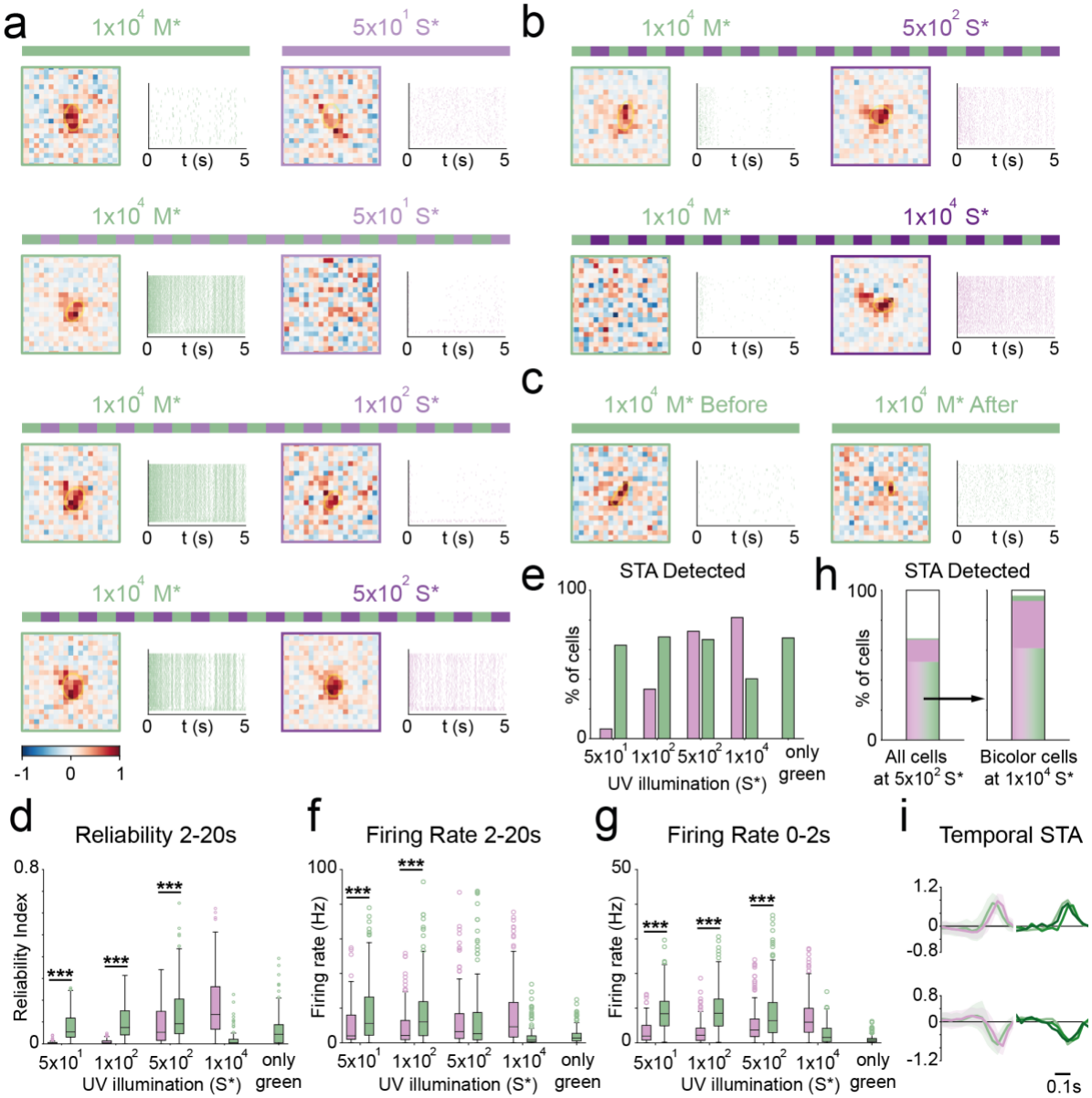

Figure 2 | Ganglion cell responses to interleaved UV-green checkerboards with varying UV intensities. a-c. Receptive fields (left) and rasters (right) obtained from the checkerboard stimuli for two example ganglion cells (Cell 1 a, Cell 2 b-c). Color bar: from dark to bright. **a.** Interleaved UV-green checkerboards. S* in the UV checkerboard is increased keeping M*=1 x 10^4 iso/ph.s constant for the green checkerboard, until reaching a close reliability in the raster responses, and a similar number of green and UV RFs (N=108 cells). **b.** Increasing S* in UV checkerboard further, up to M*/S*=1 (109 cells). **c.** Only green checkerboard comparison before and after configurations shown in b. **d.** Reliability of ganglion cell population responses to the paired interleaved UV-green checkerboards tested. (Wilcoxon signed paired test p*<0.001 for green bigger than UV). Last column corresponds to condition c.,right: only green checkerboard. The balance configuration lies above 5 x 10^2 iso/ph.s. **e.** Percentage of RFs detected for the ganglion cells tested with the different interleaved UV-green or only green checkerboards. N = 108 cells for the first two columns, 217 cells for the middle column and 109 cells for the last 2 columns. **f-g**. Firing rate of the population of cells across the paired checkerboards tested. **g.** Sustained response 2-20s. **g.** Transient response 0-2s. The balance pair is slightly below, and above 5 x 10^2 iso/ph.s respectively. **h.** Left: Percentage of ganglion cells with detected RFs for both (violet-green), single (violet or green) or none (white) of the UV-green checkerboards at S*=5 x 10^2 iso/ph.s. Right: repartition of the cells that had both RFs when the light level changed to S*=1 x 10^4 iso/ph.s. **i.** ON cells (top) and OFF cells (bottom) population average temporal STAs, normalized. Left: at S*=5 x 10^2 iso/ph.s and M*=1 x 10^4 iso/ph.s. Right: green checkerboard STAs with M*=1 x 10^4 iso/ph.s (light green), M*=1 x 10^5 iso/ph.s (green) and M*=1 x 10^6 iso/ph.s (dark green).

3.3 Reliability and firing rate decrease do not depend on recovery dynamics nor RF polarity

We wanted to understand why we retrieved less green RFs when an interleaved stimulation with high S* was present. The reason could have most likely been a reduced reliability on the responses. But, was the decrease in reliability during the green checkerboard only caused by a decrease in firing rates? To answer this, we performed a recording of an only green checkerboard right after the last color configuration of M*/S*=1. We displayed this only green checkerboard for 45 min.

Both the reliability and the sustained part of the firing rates quantified for the last green checkerboard showed strongly reduced values, compared to the ones calculated at M*/S*=20 (S*= 5 x 10^2 iso/ph.s), even if they showed a mild recovery with respect to the M*/S*=1 (S*= 1 x 10^4 iso/ph.s) (**Fig. 2d,f**). On the contrary, the firing rate of the transient response was diminished (**Fig. 2g**), probably from the now absent contribution of an offset response to UV, which was only present during the interleaved stimulation (see ON-OFF cells responses analysis below). However, the number of detected RFs returned to almost the same value found before presenting the interleaved UV-green checkerboard (**Fig. 2e**). To better understand this recovery process, we studied the evolution across time of the reliability and the detected RFs using smaller time windows to capture recovery speed (see 2.5). We observed that, regardless of the method and time window selected, there was a significant increase of the reliability across the 45 min of recording of the last, only green, checkerboard (**Fig. 3a,b)**. This recovery was slow and, as we mentioned above, did not reach the higher levels displayed in the balanced configuration within this time window. However, after a first important increase from interleaved to green only stimulation, the reliability continued to significantly increase across every time window tested. If we extrapolate this recovery using a linear approximation, we expect to attain the reliability found at the M*/S*=20 condition after 58 mins for the ganglion cells where the green RFs stayed (**Fig. 3a**), and 3hs 57 mins for the cells where the green RFs were lost (**Fig. 3b**).

Regarding the RFs detection, using also both the fixed small or the sliding and wider time windows, we saw no significant change of the percentage of ganglion cells displaying a green RF (fisher exact test p*>0.5, **Fig. 3c**). This indicates that the recovery of the cells' ability to produce a detectable RF in response to green checkerboards lied within a time window between 40s and 7 min, i.e. between the length of one sequence of the interleaved UV-green checkerboard, and the smallest time window we could use to compute an STA. Thus, the first increase in reliability recovery (**Fig. 3a**) seemed sufficient to reestablish RFs detectability in ganglion cell responses to the green checkerboard.

Next, we looked if the recovery could be quantified within the 40 s bout of the green interleaved UV-green checkerboard. In some ganglion cells, we observed a strong transitory peak response at the onset of the green checkerboard, when they were interleaved with UV checkerboards (example in **Fig. 3d**, top). After this transient peak, there was a strong decrease of the firing rate, which was present in most cells. Then, for a large fraction of the cells, there was a slow recovery of the firing rate until a steady state was reached. To see if the dynamics of this recovery is influencing the detectability of the green RFs, we quantified the recovery rate of each ganglion cell by fitting a sigmoidal curve and retrieving the

characteristic time τ it took to the cell to reach steady state (see 2.5). We discarded the first two seconds, where there is the transitory peak.

The cells displaying a quantifiable τ<40 s (50% of 109 cells) had an average value of 15.1$\pm$6.9 ms (**Fig. 3d**, bottom). We divided these cells again in two groups, cells that lost their green RF and cells that did not. We did not find any significant difference in the τ of the two groups, indicating that this recovery time was not influencing the detectability of the RF. 42% of the ganglion cells didn't show any change in firing rate (τ = 0 s), from which 22% lost the green RF, 46% kept the green RF and 32% didn't have a green RF. 8% of the ganglion cells showed a τ>40 s, meaning no recovery during the 40 s, 11% of them lose their RF, 79% of them didn't have a green RF, showing again that this recovery timescale was not impacting the reported change in reliability nor the decrease in the number of detected green checkerboard RFs.

Finally, we wondered if the strength of the transient response was influencing the reliability or the firing rate of the transient period, for the M*/S*=1 ratio. This part of the response to the green checkerboard could have two origins: one due to the onset of the green light, and the other due to the offset of the UV light from the previous sequence. To study it, we divided the cells as ON or OFF, depending on the polarity of their RF. ON cells are defined as responding to a light increase and OFF cells to a light decrease. We did this separation since we expected to find a stronger response to the UV illumination offset in OFF cells at the beginning of the green checkerboard. Indeed, they had a significantly higher firing rate compared to ON cells (**Fig. 3f**), regardless of the color of the checkerboard they responded to. This can be explained because in the majority of them (69%) an OFF cell to green light was also OFF to UV light. The transient firing rate showcased the same behavior: the OFF cells firing rates were significantly higher than the ON cells ones. However, the firing rate was significantly lower during the sustained period between 2-20 s than during the transient one (Mann Withney U double-sided test p*<0.02), as expected from the impossibility of any response to a UV offset then. We did not find any significant difference between cells of the same polarity for different colors within the transient or the sustained responses (Mann Withney U double-sided test p>0.3).

To further study if there was any influence of the firing rate of the cells on the reliability and subsequent detectability of their RF, we separated the cells into ON or OFF again, depending on their RF polarity for the UV checkerboard. We computed first the reliability ratio between the unbalanced configuration M*/S*=1 and the balanced M*/S*=20. This ratio was less than 1 for all the cells, and we found no significant differences between ON and OFF cells (**Fig. 3h**, p*>0.2). However, after comparing the decrease in reliability between the cells that lost their green RF and the ones that did not, we saw a significant decrease in the former (p*<0.05). We repeated the same analysis with the firing rate of the sustained response and we found no significant difference across ON-OFF cells and between cells that had or not their RF become undetectable (**Fig. 3i**, p>0.3).

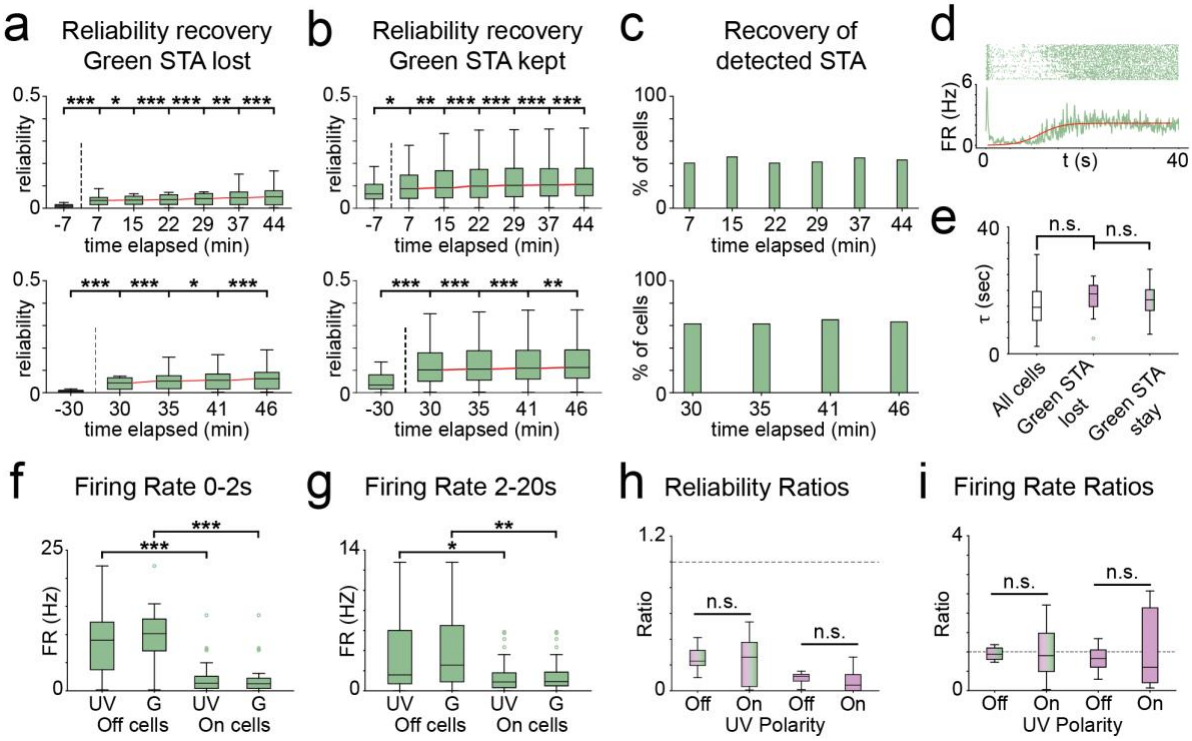

Figure 3. a-b. Reliability of ganglion cell population responses to the green checkerboard after the interleaved UV-green checkerboard at M*/S*=1. This checkerboard was divided in two ways: 1) using 6 consecutive windows of 440 s; 2) using a 1800 s sliding window with a 320 s step size. (Wilcoxon signed paired test for increase in time p<0.001 for ***, p<0.01 for ** p<0.05 for *) **a.** Reliability recovery for cells that lost their green STA between M*/S*=20 and M*/S*=1 **b.** Reliability recovery for cells that kept their green STA **c.** Detected STA recovery **d.** Example firing rate and histogram for the green checkerboard of a ganglion cell **e.** τ population responses shown with box plots, separating ganglion cells with detected and undetected green RFs. Differences between groups is not significant (Mann Withney U test p*<0.3). **f-g.** Firing rate of green checkerboard during the interleaved UV-green checkerboard at M*/S*=1 as a function of green or violet polarity. (Mann Whitney U double-sided test p*<0.001) **f.** Transient firing rate (0-2s) **g.** Sustained firing rate (2-20s) **h.** Reliability ratios responses to the green checkerboard between M*/S*=1 and M*/S*=20 (Mann Whitney U double-sided test p*>0.05) **i.** Firing rate ratios

3.4 High frequency responses to full field interleaved UV-green color chirps also have an S*-M* optimal balance

In the previous section we found a striking reduction in the reliability of the response to green checkerboards when we interleaved UV-green checkerboards with sufficiently high S*. This produced a decrease in the capability of ganglion cells to reliably respond to fine spatial details, thus preventing the detection of RFs. However, the sustained responses did not diminish as strongly, and they remained comparable between the cells that had a detectable RF and the cells that did not. We wondered then if a similar behaviour could be found for the finer temporal details in the ganglion cells response to full field interleaved stimulations. For this, we decided to use chirp stimulations, since these are typically used to characterize the responses of ganglion cells and classify them into different cell types (Baden et al., 2016; Gonschorek et al. 2025). This stimulus is 32 s long and contains the typical components used in many studies using color: ON and OFF steps of full field light, allowing us to compare our results with other works.

We can divide the chirp stimulus into two regimes, first 0-7 s corresponding to light on and off steps, and the range between 9-27 s corresponding to a fast modulation of the frequency and the amplitude (see stimulus profile, **Fig. 4a**, top). The protocol applied here was identical to the one we used for the checkerboards, with an extra intensity value at S*=1 x 10^3 iso/ph.s. Similar to what we described for the color illuminated checkerboards, the green chirp displayed a reliable response that faded away when S* was increased, reaching very low firing rate values (**Fig. 4a**). The opposite behavior was seen for the responses to UV chirps, as both the reliability and firing rate increased with increasing S*. In the same fashion as with the interleaved green checkerboards, the step responses were not fully abolished, even if for the green chirps these step responses were separated from the previous UV chirp stimulation by a period of dark full field of 4 s. The responses to green stimulation were recovered right after the end of the interleaved UV-green chirp, when we displayed a green-only chirp (**Fig. 4b**). This recovery was much larger for the fast varying portion than for the steps.

When studying the responses to the ON-OFF steps portion of the chirp, we found that their reliability in the UV condition increased with the S*. An equivalence in reliability to the UV and green conditions was found at the same ratio as with the interleaved UV-green checkerboards, i.e. at M*/S*=20 (N= 149 cells, **Fig. 4c**). With the added S* value of 1 x 10^3 iso/ph.s, corresponding to M*/S* = 10, we determined a higher threshold for the balance configuration, since the green chirp response reliability already showed a decrease. When quantifying the reliability to the fast modulation portion of the chirp, we saw that the balanced ratio appeared for values below S*=5 x 10^2 iso/ph.s, i.e. for higher values than M*/S*= 20 (**Fig. 4d**). For both portions of the chirp we saw a recovery of the reliability when stimulating with an only green chirp right afterwards (**Fig. 4c-d**, last column).

Regarding the firing rates of the ganglion cells to both the step and the fast modulation regions of the chirps, we saw that they stopped being significantly lower in response to UV chirps than to green chirps when the M*/S*=20 configuration was reached, as S* increased (**Fig. 4e-f**). In both cases, at this M*/S* ratio, we can see that the difference in firing rate between the response to green and the response to UV is not big. These results showed similar behavior in the ganglion cell responses to interleaved UV-green chirps and checkerboards, highlighting the interaction between the two colors on ganglion cell responses, with S* having a strong impact on the reliability of the responses to green color, both for fine spatial and fast temporal features.

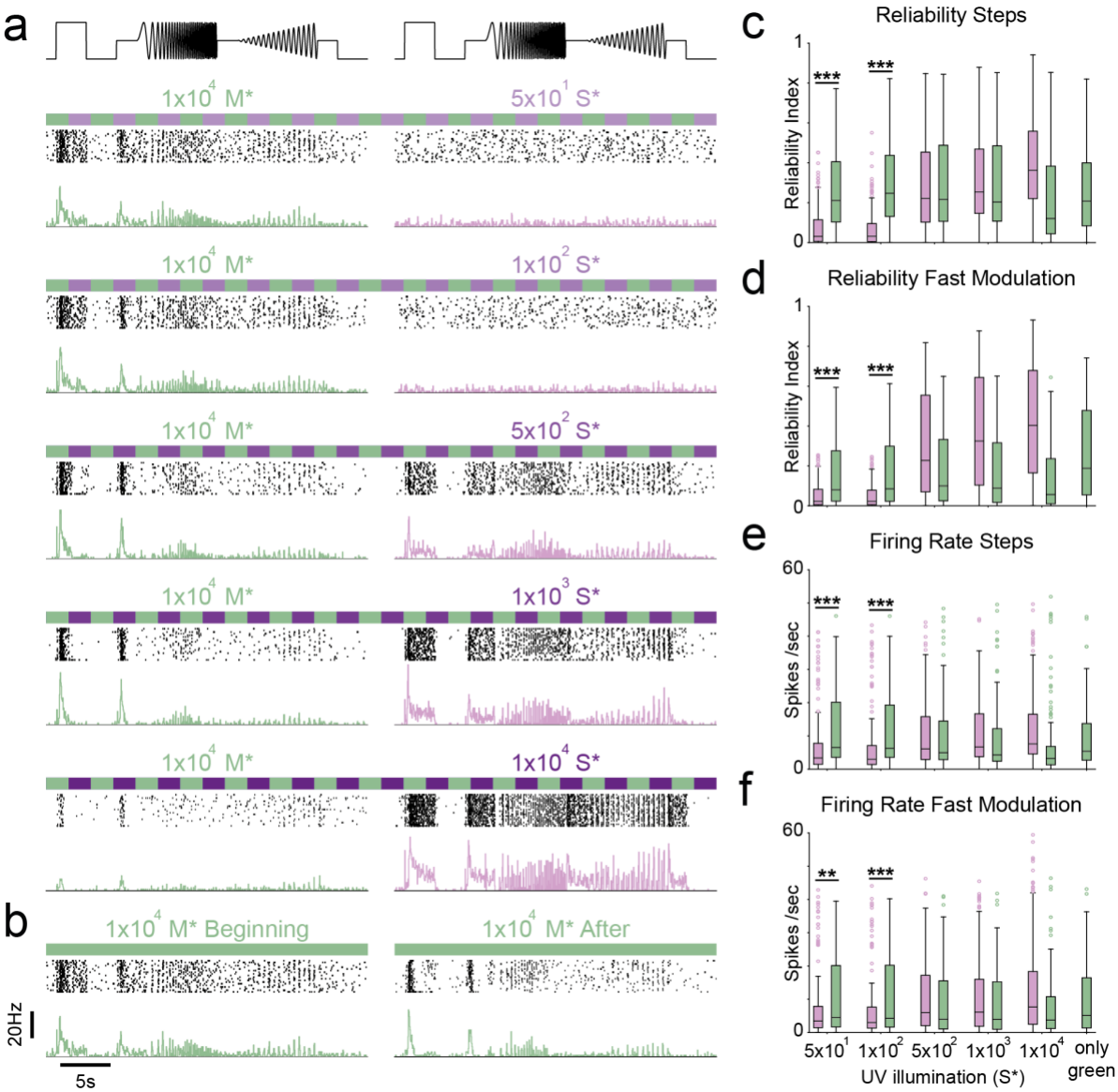

Figure 4 | Ganglion cell responses to two-color interleaved chirps with varying UV intensities. a-b. Response of an example ON ganglion cell to the interleaved full field color illuminated chirp stimulus. Top: raster, bottom: firing rate. Left: green, Right: violet. **a.** Increasing S* in UV chirps up to M*/S*=1, with constant M*=1 x 10^4 io/ph.s (149 cells). **b.** Only green chirp comparison in the beginning and after configurations shown in a **c-d.** Reliability of ganglion cell population responses to the paired UV and green interleaved chirps tested. (Wilcoxon signed paired test p*<0.001 for green bigger than UV). Last column corresponds to condition b.: only green checkerboard. **c.** Steps region: 0-7 s. The balance configuration is at 5 x 10^2 iso/ph.s.(149 cells). Wilcoxon paired test (p<0.001 for ***, p<0.05 for *). **d.** Fast modulated region: 9-27 s. The balance configuration is below 5 x 10^2 iso/ph.s.(149 cells). Wilcoxon paired test (p< 0.001 for ***, p<0.05 for *) **e-f**. Firing rate of the population of cells across the paired chirps tested. The balance pair is slightly below 5 x 10^2 iso/ph.s. **e.** Steps responses 0-7s. **f.** Fast modulation responses 9-27s.

3.5 The natural S*-M* ratio of light arriving to mice retina lies close to a balanced ratio

So far, we studied the responses of retinal ganglion cells to interleaved color stimulations with fine spatial details using checkerboards, and to fast full field modulations in intensity using chirps. The light intensity values we tested indicated that M*/S* = 20 was close to where the reliability to both UV and green stimulations was balanced, for the 40 and 32 s

interleaved bouts of color stimuli tested. This value also allowed for a balance in the number of RFs detected during checkerboard stimulation to be reached. Concerning the firing rates, we found that the balance was achieved between the ratios M*/S*=100 and M*/S*=20. We thus decided to use a mid value of M*/S*=60 as a higher cut for finding balanced responses. For the lower cut, we chose a value of M*/S*=10, which we tested for chirps and was close to eliciting a balance too.

We arrive to an approximate range of 10<M*/S*<60 that supports a balanced reliability and similar firing rate responses to both the UV and green portions of the stimuli (see Discussion for rhodopsin treatment). With this in mind, we wondered if these ratios could be achieved using a unique light wavelength, as it could be the case in many laboratory experimental settings (see 2.9). We see that a single source of narrow monochromatic light with a peak wavelength between $431\ nm < L < 444\ nm$ achieves a balanced-inducing illumination (**Fig. 5a**). However, labs have access to very different kinds of broadly available LEDs. These lights are usually called "white" and are standardized to have an equivalent "temperature" (Kokka et al., 2018). They present a broad spectrum and often a major peak in both a low and a high wavelength ranges (**Fig. 5a**).

The illumination levels and spectra we use in our experiments are artificial and mice may not find them in natural environments. We quantified then the M*/S* ratio that mice will be confronted to when outside of controlled laboratory conditions. To calculate this, we analysed the spectral content of light in natural conditions, taking into account two variables (**Fig. 5b**). First, the eye ocular media absorption spectrum, that depends on λ (Henrikson et al., 2010), showing a strong attenuation of the mouse eye's transmission in UV, which is the case for many other species (Douglas & Jeffery, 2014). Second, the natural spectral content that may change across the time of the day (Yu et al., 2023). The spectra measured were taken at around 1 meter height, with the light sensor facing up, and the recordings were done starting after sunrise and ending before sunset, with a clear ("sunny") sky. Even if this is not the exact situation a mouse will encounter in nature, it is close to the spectra coming from the sky, which would arrive at the ventral part of the retina, from which we recorded in our work.

With these data, we could calculate the S- and M-opsin isomerisation rates that mice would experience in this natural environment at different times of the day (**Fig. 5c**) (see 2.9). The data showed a linear relationship, giving a fitted M*/S*=9.8 ratio (R^2 = 0.9). These pseudo-natural rates calculated for the mice retina across different times of the day fall close or inside the region of balanced responses (**Fig. 5c**, gray area), while the unbalanced ones lie much further away .

To verify this alignment was not merely a coincidence, we performed another experiment, but at a much higher photopic level. Starting with a constant value M*=1.9x10^6 we increased the S* as we did before, until reaching a balanced configuration. We did this additional experiment only using chirp stimuli. We found that the balanced ratio was M*/S*=29, with S*=6.4x10^4 iso/ph.s. (**Fig. 5c**, blue cross). This point lies within the gray area defined above, and is closer to the natural daylight data than to the M*/S*=1 ratio (**Fig. 5c**, red dashed line) and near the ratio of M*/S*=20 (**Fig. 5c**, green dashed line). Therefore, the region of balanced ganglion cells responses we empirically found with our experiments lies

close to the isomerisation rate ratios the mouse retina may encounter during daylight.

Finally, we asked if the LED lights commercially available are useful in a laboratory setting to probe the mice retina mimicking natural illumination conditions. We see that, on the contrary to a ratio of M*/S*=1, these LEDs will elicit a much higher isomerisation rate for M-opsin than for S-opsin, close to the high unbalanced situation we tested here with low S*=50 iso/ph.s and M*=1 x 10^4 iso/ph.s (**Fig. 5c**, cyan to violet lines). These LED lights are thus eliciting much more activity in the ganglion cells coming from M-opsin activation than from S-opsin.

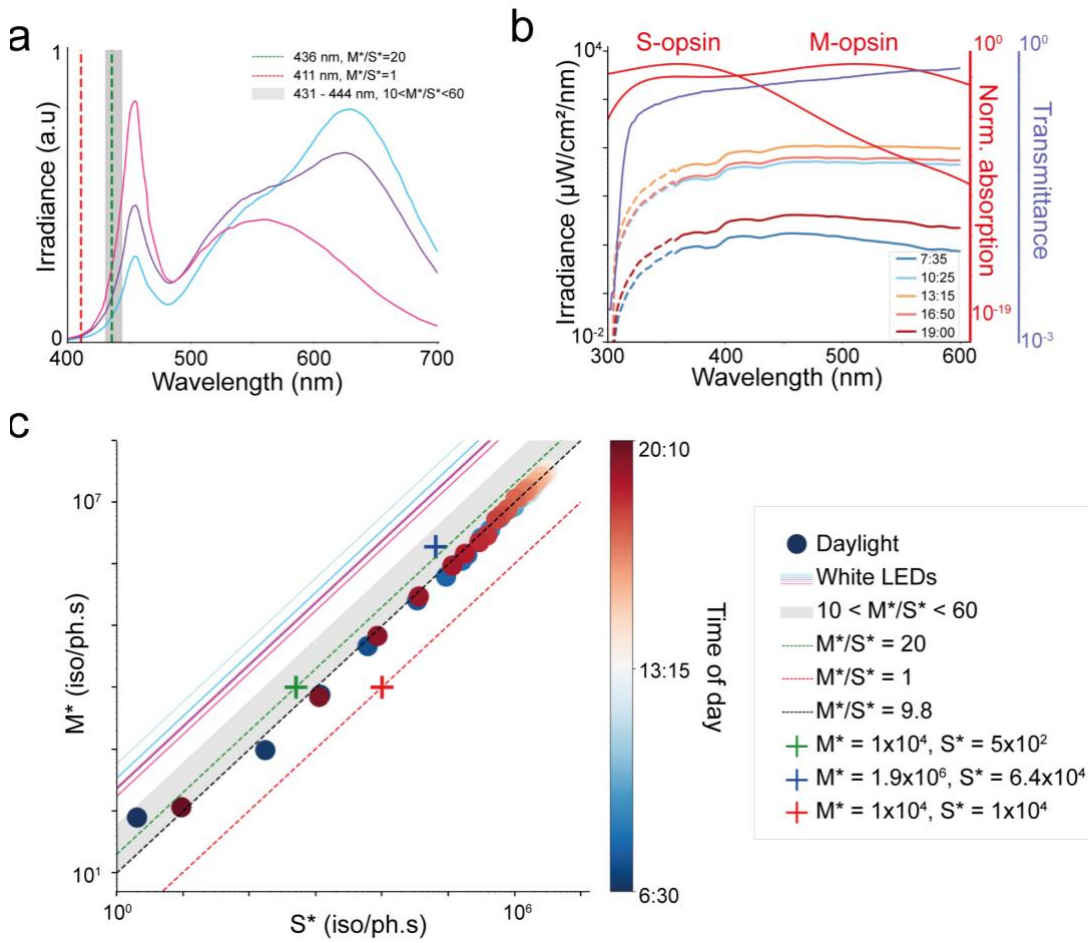

Figure 5 | A balance M*-S* isomerisation rate ratio is close to the natural daylight illumination ratio. a. An ideal monochromatic light source ($\sigma = 0.01\ nm$) that produces an M*/S*=1 ratio (red), at a peak wavelength of 411 nm, a M*/S*=20 ratio (green), at a peak wavelength of 436 nm, a region where these sources produce 10<M*/S*<60 (grey), at peak wavelengths between 431 nm and 444 nm, and the normalized irradiance spectra of commercial white LEDS for low (cyan), medium (violet) and high (pink) temperature illumination. **b.** Spectral transmittance of the ocular media of mice before light reaches the retina (purple) together with the measured spectra of natural light at different times of the day (blue to red curves, Henrikson et al., 2010) are overlaid with the absorption curves of S- and M-opsins. The natural light's spectra have been extended towards short wavelengths (dashed part of the curves, see 2.9). **c.** M* vs S* iso/ph.s representations of balanced responses configurations found (green and blue crosses), and unbalanced ones (red cross). The balance 10<M*/S*<60 ratio region is shaded. Dashed lines represent constant M*/S* ratios. White LEDs' are represented with full lines, having temperatures of: 2400, 2700, 3000, 4000, 5000 and 6500 K (cyan to pink,Kokka et al., 2018).

4. Discussion

Our experiments revealed a significant cross-talk between the S-opsin (UV) and M-opsin (green) information processing channels in the mouse retina. S-opsin activation strongly influences ganglion cell responses to green light, which elicits mainly M-opsin activation. High M*/S* ratios during green-UV interleaved light stimulation produce a suppression of ganglion cell responses to green light. This effect is impacting the capability of ganglion cells to respond reliably to small spatial features (**Fig 2**) or to fast temporal fluctuations (**Fig 4**). We did our experiments in the near-photopic level of M*=1 x 10^4 iso/ph.s, and we confirmed that at a higher photopic level of M*=1.8x10^6 iso/ph.s a balanced M*/S* ratio also falls within the same region we determined (**Fig 5**). We showed that the naturally occurring mesopic/photopic daylight illumination conditions reaching the retina of mice from dawn to dusk produces an approximate constant isomerisation rate ratio near M*/S*=10, which lies on the limit of the balance range we found empirically. This finding is in accordance with an information theoretical approach (Barlow, 1961), where it is suggested that to efficiently encode information, sensory relays need to be specifically tuned to the stimulus they want to encode (having a M*/S* encoding ratio near the natural one).

To elicit comparable ganglion cell responses, a 1 to 2 orders of magnitude for M* to S* is required. This disparity suggests that UV-activated pathways undergo a different amplification mechanism compared to green-activated ones, which is witnessed by a higher sensitivity at shorter wavelengths (Jacobs, Neitz, Deegan, 1991). Previous works have also shown the suppression of responses to green at high isomerisation rates using achromatic light, and argued that this is due to signals coming from the rod pathway which reaches saturation and stops responding (Joesch & Meister, 2016; Nikonov et al., 2006). Although there may be some rod contribution to green light responses, and it has been shown that rods can escape saturation (Adelson, 1982; Khani & Gollisch, 2021), this is not the effect we show here for the 52% of the ganglion cells that show responses to both UV and green illumination. At the ratio of M*/S*=20, our interleaved UV illumination only elicits M*=1.2 x 10^2 iso/ph.s, and our green light kept M* constant at least two orders of magnitude above, together with R* in close to saturation levels (2 x 10^4 iso/ph.s).

Two observations suggest that the biggest contribution to the responses we measured in response to green stimuli come from M-opsin cone activation and not from rods. First, the temporal RFs responses were fast for the green checkerboards, while it is known that they should be much slower for rhodopsin inputs. When stimulating with UV light, activating mostly S-opsin cone pathways, mice ganglion cell responses are typically faster, similarly to those of primate ganglion cells to visible light (Demb, Singer, 2015; Wang et al., 2011; Borghuis et al., 2014). The responses we recorded had similar latencies for both the UV and green checkerboard, and they did not change even when we increased the luminance to reach bleaching levels for rhodopsin (**Fig. 2h**). Second, we measured only 1 color opponent cell out of 217 cells, looking only at their RF polarity. It has been shown that color opponency in mice is mainly driven by an S-opsin/rhodopsin input coming through lateral feedback from horizontal cells (Joesch & Meister, 2016; Szatko et al., 2020). Horizontal cells can form a dense, electrically coupled network (Baden & Osorio, 2019; Becker et al., 1998; Cook & Becker, 1995) that interacts with photoreceptors via lateral inhibition. In our experiment, only the ganglion cells that displayed only green RFs were unaffected by the interleaved UV

light. This suggests a mechanism by which both S-opsin and M-opsin inputs converge at a lower processing stage in the retinal circuit, or happen to be processed from co-expression of S- and M-opsin within the same cone (Szel et al., 1992; Haverkamp et al., 2005).

Different dynamics of recovery are found in the retina, and we have also found recovery of ganglion cells responses at different timescales. First, during an interleaved green-UV checkerboard at a ratio of M*/S* = 1, we saw in some cells that the firing rate in response to green stops and recovers in 10-40 s. Second, after the end of this interleaved checkerboard, the detected STA recovers in minutes (1-7 min) but the reliability takes longer to recover (1-4 h). In the same way, photoreceptors are capable of reacting at multiple timescales. Fast dynamics were found when modeling photoreceptors adaptation mechanisms (1-10 ms, Angueyra et al., 2022; Idrees et al., 2024). These photoreceptor models, which capture key biophysical mechanisms, improved predictions of retinal responses to natural stimuli across wide isomerisation rate changes. On the other extreme, dark adaptation takes 3 hours to span 5 orders of magnitude in light sensitivity in cats (Barlow et al., 1957). Another slow adaptation is the recovery of sensitivity to bright light after dim light exposure, due to rapid photopigment breakdown, causing bleaching and glare (Cornwall et al., 1990). These two types of adaptation were not present in our study. Our detected STA recovery time seems compatible with the timescale reported in human psychophysics experiments related to color persistence (Gupta et al., 2020). This effect is called “chromatic adaptation”, and it consists of the human visual system’s capability to adjust to widely varying colors of illuminants in order to approximately maintain the consistency of perceived color appearance. The time course of chromatic adaptation can be divided into 3 stages: an extremely fast, a fast and a slower stage (Fairchild and Reniff. 1995; Rinner and Gegenfurtner. 2000). It was found that the slow chromatic adaptation reaches 80–90% within a minute and is complete after five minutes. Further work is needed to determine if the timescale we measured here in mice, and the slow adaptation required for the colour constancy to stabilize in humans, are produced by the same mechanisms.

Future studies may explore smaller time intervals in between color interleaved stimulations, to see if our results hold for intervals below 40 s / 32 s. It could be interesting to see if the effect disappears in a continuous manner, if there is a fast transition, or if it remains the same. This can be achieved using two projectors, one for each color, as shown in our work or in this study (Franke, Chagas et al., 2019). This will allow us to better understand the computations of the ganglion cells, and of the retina in general. Simultaneous two-color light stimulation may reveal on the other hand strong nonlinear interactions, at least for the transient responses lasting up to several hundreds of milliseconds. (Khani & Golliisch, 2021). Therefore, studies using linear decorrelation to extract the contributions of one opsin from the other to the responses could have a bias due to the non-linearity of color processing in the retina.

Regarding the number of responding cells, our work may explain the strong unbalance found in previous works between the number of ganglion cells presenting a center RF for UV light compared to green light in the ventral retina (Szatko et al., 2020). It could also explain why there are more amacrine cell classes found tuned to UV compared to green (Korympidou et al., 2020). This effect could be due to the M*/S*=1 isomerisation rate ratio used in these studies. We have witnessed in our work a decrease in 60% of the ganglion cells

displaying a green RF when arriving to this ratio, from the balance ratio of M*/S*=20 (**Fig. 2e**). The balanced ratio found in our work highlights the complexity of color processing in the retina and the necessity of fine-tuning stimulus spectral content and intensity to accurately study color interactions in visual processing. Our checkerboard stimulus is tailored to study small spatial details and extract RFs, so it does not invalidate that color opponency in mice is present mostly in the cells of the ventral retina. However it may change the view in which the ventral retina of mice is mostly dedicated to S-opsin signal processing, since M-opsin responses appear widespread through the ganglion cells we recorded.

Previous works used "white" or 415 nm LED to illuminate the mouse retina for different stimuli. We saw here that using these types of illuminations will not create a M*/S* ratio found in natural conditions. On the one hand, a "white" LED will have a M*/S* ratio superior to the natural ratio, causing the retina to process only the green inputs. Using a single color LED that has a M*/S* < 10 will cause the retina to process only the violet inputs. Thus, a bias towards studying only the cells not abolished by UV light or by green light is likely to be present in previous studies, depending on the type of illumination used. A solution for this is either to calibrate the intensity of two or more light sources to attain a balance M*/S*, or to buy a single blue light source that achieves this (**Fig. 5a**).

Regarding fast varying temporal responses, we attained the same balanced responses with a natural M*/S* ratio (**Fig 5c**). For the ON and OFF steps some green responses stayed, even at a lower M*/S* ratio. We don't know if this is enough to study the smaller spatial details of fast varying natural scenes. This information may not be used effectively by mice, or it could be relevant for their natural behavior in natural illumination conditions. Recent works have explored the retina and V1 responses to color movies (Franke et al., 2022). These movies were taken with a novel camera that measured precisely the spectral content of the natural habitat of mice (Qiu et al., 2021). However, if these movies are presented with a unnatural ratio of M*/S*, it could create a bias and unnatural shift of the responses to only the UV illumination channel. On the other hand, the balanced ratio we obtained at a high mesopic/photopic regime could seem unnatural for mice which are typically regarded as strictly nocturnal. However they often forage during the day in the wild (Daan et al., 2011). Thus, studying the natural illumination from dawn to dusk, from mesopic to photopic may be interesting to understand the way mice use their S- and M- cones in a natural setting.

In conclusion, our findings highlight the need for a precise color illumination balance in photopic conditions when studying small spatial and fast temporal color response features in ganglion cells. This will place the retina into a close to naturally occurring illumination condition, which allows the M- and S-opsin information to arrive simultaneously, and with the same reliability, to the majority of the ganglion cells in the ventral retina. In future studies that explore the responses to color natural images or videos, maintaining a proper color balance will be essential. It will help disambiguate from an instantaneous nonlinear color interaction, when two colors are presented simultaneously, from the long lasting effects we show here, ensuring a more accurate interpretation of ganglion cell responses, and retinal processing in general. It is crucial to balance the stimulus intensities to avoid misinterpreting the color interactions in retinal visual processing. This has broader implications not only for retinal studies but also for understanding color vision in other species and in the context of color vision restoration efforts (Bansal et al., 2024). Future

research should consider these factors when designing experiments and interpreting data, particularly when exploring visual processing of complex, dynamic color scenes.

Data statement

Data will be made available upon publication.

Acknowledgements

We would like to thank Olivier Marre for helpful discussions. This work was funded by Agence Nationale de la Recherche grants ANR-23-CE37-0004-01 HiDeepID, ANR-22-CE37-0016-01 PerBaCo, ANR-21-CE37-0024 NatNetNoise, by IHU FOReSIGHT (ANR-18-IAHU-01) and by Sorbonne Center for Artificial Intelligence-Sorbonne UniversityIDEX SUPER 11-IDEX-0004. This work has been done within the framework of the PostGenAI@Paris project and it has benefitted from financial support by the Agence Nationale de la Recherche (ANR) with the reference ANR-23-IACL-0007. Our lab is part of the DIM C-BRAINS, funded by the Conseil Régional d'Ile-de-France.

Author contributions

FC, AL, TQ and RB performed experiments. FC, AL, TQ, UF and MG analyzed the data. MG wrote the manuscript with input from all authors. MG and UF conceptualized the work. MG supervised the work. MG and UF secured funding.

References

Adelson, E.H., 1982. Saturation and adaptation in the rod system. Vision research, 22(10), pp.1299-1312.

Allen, A.E., Storchi, R., Martial, F.P., Petersen, R.S., Montemurro, M.A., Brown, T.M., Lucas, R.J., 2014. Melanopsin-Driven Light Adaptation in Mouse Vision. Current Biology, 24(21), pp. 2481–2490.

Angueyra, J.M., Baudin, J., Schwartz, G.W. and Rieke, F., 2022. Predicting and manipulating cone responses to naturalistic inputs. Journal of Neuroscience, 42(7), pp.1254-1274.

Atick, J.J., Li, Z. and Redlich, A.N., 1992. Understanding retinal color coding from first principles. Neural computation, 4(4), pp.559-572.

Baden, T., Berens, P., Franke, K., Román Rosón, M., Bethge, M. and Euler, T., 2016. The functional diversity of retinal ganglion cells in the mouse. Nature, 529(7586), pp.345-350.

Baden, T., Osorio, D., 2019. The Retinal Basis of Vertebrate Color Vision. Annual Review of Vision Science, 5(Volume 5, 2019), pp. 177–200.

Baden, T., 2020. Vertebrate vision: Lessons from non-model species. Seminars in Cell & Developmental Biology, 106, pp.1–4.

Baden, T., Euler, T. and Berens, P., 2020. Understanding the retinal basis of vision across species. *Nature Reviews Neuroscience*, *21*(1), pp.5-20.

Baden, T., 2024. Ancestral photoreceptor diversity as the basis of visual behaviour. Nature Ecology & Evolution, 8(3), pp.374-386.
Bansal, H., Pyari, G., Roy, S., 2024. Theoretical prediction of broadband ambient light optogenetic vision restoration with ChRmine and its mutants. Scientific Reports, 14(1), p. 11642.
Barlow, H.B., Fitzhugh, R., Kuffler, S.W., 1957. Change of organization in the receptive fields of the cat's retina during dark adaptation. The Journal of physiology, 137(3), p. 338.
Barlow, H.B., 1961. Possible principles underlying the transformation of sensory messages. Sensory communication, 1(01), pp. 217–233.
Becker, D., Bonness, V., Mobbs, P., 1998. CELL COUPLING IN THE RETINA: PATTERNS AND PURPOSE. Cell Biology International, 22(11), pp. 781–792.
Behrens, C., Schubert, T., Haverkamp, S., Euler, T. and Berens, P., 2016. Connectivity map of bipolar cells and photoreceptors in the mouse retina. Elife, 5, p.e20041.
Borghuis, B.G., Looger, L.L., Tomita, S., Demb, J.B., 2014. Kainate Receptors Mediate Signaling in Both Transient and Sustained OFF Bipolar Cell Pathways in Mouse Retina. Journal of Neuroscience, 34(18), pp. 6128–6139.
Breuninger, T., Puller, C., Haverkamp, S. and Euler, T., 2011. Chromatic bipolar cell pathways in the mouse retina. Journal of Neuroscience, 31(17), pp.6504-6517.
Cook, J.E., Becker, D.L., 1995. Gap junctions in the vertebrate retina. Microscopy Research and Technique, 31(5), pp. 408–419.
Cornwall, M.C., Fein, A., MacNichol, E.F., Jr, 1990. Cellular mechanisms that underlie bleaching and background adaptation. Journal of General Physiology, 96(2), pp. 345–372.
Daan, S., Spoelstra, K., Albrecht, U., Schmutz, I., Daan, M., Daan, B., Rienks, F., Poletaeva, I., Dell'Omo, G., Vyssotski, A., Lipp, H.-P., 2011. Lab Mice in the Field: Unorthodox Daily Activity and Effects of a Dysfunctional Circadian Clock Allele. Journal of Biological Rhythms , 26(2), pp. 118–129.
Dacey, D.M., 1996. Circuitry for color coding in the primate retina. Proceedings of the National Academy of Sciences, 93(2), pp.582-588.
Dacey, D.M., 1999. Primate retina: cell types, circuits and color opponency. Progress in retinal and eye research, 18(6), pp.737-763.
Demb, J.B., Singer, J.H., 2015. Functional Circuitry of the Retina. Annual Review of Vision Science, 1(Volume 1, 2015), pp. 263–289.
Denman, D.J., Luviano, J.A., Ollerenshaw, D.R., Cross, S., Williams, D., Buice, M.A., Olsen, S.R. and Reid, R.C., 2018. Mouse color and wavelength-specific luminance contrast sensitivity are non-uniform across visual space. elife, 7, p.e31209.
Doi, E., Inui, T., Lee, T.W., Wachtler, T. and Sejnowski, T.J., 2003. Spatiochromatic receptive field properties derived from information-theoretic analyses of cone mosaic responses to natural scenes. Neural computation, 15(2), pp.397-417.
Douglas, R.H., Jeffery, G., 2014. The spectral transmission of ocular media suggests ultraviolet sensitivity is widespread among mammals. Proceedings of the Royal Society B: Biological Sciences, 281(1780), p. 20132995.
Estévez, O., Spekreijse, H., 1982. The "silent substitution" method in visual research, *Vision Research*, 22(6), pp. 681–691.
Euler, T., Hausselt, S.E., Margolis, D.J., Breuninger, T., Castell, X., Detwiler, P.B., Denk, W., 2009. Eyecup scope—optical recordings of light stimulus-evoked fluorescence

signals in the retina. *Pflügers Archiv - European Journal of Physiology*, 457(6), pp. 1393–1414.
Euler, T., Franke, K. and Baden, T., 2019. Studying a light sensor with light: multiphoton imaging in the retina. *Multiphoton Microscopy*, pp.225-250.
Fairchild, M.D., Reniff, L., 1995. Time course of chromatic adaptation for color-appearance judgments, *JOSA A*, 12(5), pp. 824–833.
Fornetto, C., Euler, T., Baden, T., 2024. Vertebrate vision is ancestrally based on competing cone circuits. bioRxiv, p. 2024.11.19.624320.
Field, G.D., Gauthier, J.L., Sher, A., Greschner, M., Machado, T.A., Jepson, L.H., Shlens, J., Gunning, D.E., Mathieson, K., Dabrowski, W. and Paninski, L., 2010. Functional connectivity in the retina at the resolution of photoreceptors. Nature, 467(7316), pp.673-677.
Franke, K., Maia Chagas, A., Zhao, Z., Zimmermann, M.J., Bartel, P., Qiu, Y., Szatko, K.P., Baden, T. and Euler, T., 2019. An arbitrary-spectrum spatial visual stimulator for vision research. elife, 8, p. e48779.
Franke, K., Willeke, K.F., Ponder, K., Galdamez, M., Zhou, N., Muhammad, T., Patel, S., Froudarakis, E., Reimer, J., Sinz, F.H. and Tolias, A.S., 2022. State-dependent pupil dilation rapidly shifts visual feature selectivity. Nature, 610(7930), pp.128-134.
Franke, K., Cai, C., Ponder, K., Fu, J., Sokoloski, S., Berens, P. and Tolias, A.S., 2023. Asymmetric distribution of color-opponent response types across mouse visual cortex supports superior color vision in the sky. *bioRxiv*, pp.2023-06.
Goethals, S., Louboutin, A., Hamlaoui, S., Quetu, T., Virgili, S., Goldin, M.A., Baranton, K. and Marre, O., 2024. Nonlinear spatial integration allows the retina to detect the sign of defocus in natural scenes. bioRxiv, pp.2024-06.
Goldin, M.A., Lefebvre, B., Virgili, S., Pham Van Cang, M.K., Ecker, A., Mora, T., Ferrari, U. and Marre, O., 2022. Context-dependent selectivity to natural images in the retina. Nature Communications, 13(1), p.5556.
Goldin, M.A., Virgili, S. and Chalk, M., 2023. Scalable gaussian process inference of neural responses to natural images. Proceedings of the National Academy of Sciences, 120(34), p.e2301150120.
Gonschorek, D., Goldin, M.A., Oesterle, J., Schwerd-Kleine, T., Arlinghaus, R., Zhao, Z., Schubert, T., Marre, O. and Euler, T., 2025. Nitric oxide modulates contrast suppression in a subset of mouse retinal ganglion cells. *eLife*, *13*, p.RP98742.
Govardovskii, V.I., Fyhrquist, N., Reuter, T.O.M., Kuzmin, D.G. and Donner, K., 2000. In search of the visual pigment template. Visual neuroscience, 17(4), pp.509-528.
Gupta, G., Gross, N., Pastilha, R., Hurlbert, A., 2020. The time course of chromatic adaptation under immersive illumination. bioRxiv, p. 2020.03.10.984567
Gupta, D., Młynarski, W., Sumser, A., Symonova, O., Svatoň, J. and Joesch, M., 2023. Panoramic visual statistics shape retina-wide organization of receptive fields. Nature Neuroscience, 26(4), pp.606-614.
Haverkamp, S., Wässle, H., Duebel, J., Kuner, T., Augustine, G.J., Feng, G., Euler, T., 2005. The Primordial, Blue-Cone Color System of the Mouse Retina. Journal of Neuroscience, 25(22), pp. 5438–5445.
Henriksson, J.T., Bergmanson, J.P.G., Walsh, J.E., 2010. Ultraviolet radiation transmittance of the mouse eye and its individual media components. Experimental Eye Research, 90(3), pp. 382–387.

Höfling, L., Szatko, K.P., Behrens, C., Deng, Y., Qiu, Y., Klindt, D.A., Jessen, Z., Schwartz, G.W., Bethge, M., Berens, P. and Franke, K., 2024. A chromatic feature detector in the retina signals visual context changes. *Elife*, *13*, p.e86860.
Idrees, S., Manookin, M.B., Rieke, F., Field, G.D. and Zylberberg, J., 2024. Biophysical neural adaptation mechanisms enable artificial neural networks to capture dynamic retinal computation. Nature Communications, 15(1), p.5957.
Jacobs, G.H., Neitz, J., Deegan, J.F., 1991. Retinal receptors in rodents maximally sensitive to ultraviolet light, *Nature*, 353(6345), pp. 655–656.
Jacobs, G.H., Williams, G.A., Fenwick, J.A., 2004. Influence of cone pigment coexpression on spectral sensitivity and color vision in the mouse. Vision Research, 44(14), pp. 1615–1622.
Joesch, M. and Meister, M., 2016. A neuronal circuit for colour vision based on rod–cone opponency. Nature, 532(7598), pp.236-239.
Karamanlis, D., Schreyer, H.M. and Gollisch, T., 2022. Retinal encoding of natural scenes. Annual Review of Vision Science, 8(1), pp.171-193.
Khani, M.H. and Gollisch, T., 2021. Linear and nonlinear chromatic integration in the mouse retina. Nature communications, 12(1), p.1900.
Kokka, A., Poikonen, T., Blattner, P., Jost, S., Ferrero, A., Pulli, T., Ngo, M., Thorseth, A., Gerloff, T., Dekker, P., Stuker, F., Klej, A., Ludwig, K., Schneider, M., Reiners, T., Ikonen, E., 2018. Development of white LED illuminants for colorimetry and recommendation of white LED reference spectrum for photometry. Metrologia, 55(4), p. 526.
Korympidou, M.M., Strauss, S., Schubert, T., Franke, K., Berens, P., Euler, T., Vlasits, A.L., 2024. GABAergic amacrine cells balance biased chromatic information in the mouse retina. Cell Reports, 43 (11).
Maheswaranathan, N., McIntosh, L.T., Tanaka, H., Grant, S., Kastner, D.B., Melander, J.B., Nayebi, A., Brezovec, L.E., Wang, J.H., Ganguli, S., Baccus, S.A., 2023. Interpreting the retinal neural code for natural scenes: From computations to neurons. Neuron, 111(17), pp. 2742-2755.e44.
McIntosh, L., Maheswaranathan, N., Nayebi, A., Ganguli, S., Baccus, S., 2016. Deep learning models of the retinal response to natural scenes. Advances in neural information processing systems, 29.
Mouland, J.W., Pienaar, A., Williams, C., Watson, A.J., Lucas, R.J. and Brown, T.M., 2021. Extensive cone-dependent spectral opponency within a discrete zone of the lateral geniculate nucleus supporting mouse color vision. Current biology, 31(15), pp.3391-3400.
Nikonov, S.S., Kholodenko, R., Lem, J. and Pugh Jr, E.N., 2006. Physiological features of the S-and M-cone photoreceptors of wild-type mice from single-cell recordings. The Journal of general physiology, 127(4), p.359.
Osorio, D., Smith, A.C., Vorobyev, M. and Buchanan-Smith, H.M., 2004. Detection of fruit and the selection of primate visual pigments for color vision. The American Naturalist, 164(6), pp.696-708.
Pearson, J.T., Kerschensteiner, D., 2015. Ambient illumination switches contrast preference of specific retinal processing streams. Journal of Neurophysiology, 114(1), pp. 540–550.
Peichl, L., 2005. Diversity of mammalian photoreceptor properties: adaptations to habitat and lifestyle?. The Anatomical Record Part A: Discoveries in Molecular, Cellular, and Evolutionary Biology: An Official Publication of the American Association of Anatomists, 287(1), pp.1001-1012.

Peichl, L., Kaiser, A., Rakotondraparany, F., Dubielzig, R.R., Goodman, S.M. and Kappeler, P.M., 2019. Diversity of photoreceptor arrangements in nocturnal, cathemeral and diurnal Malagasy lemurs. Journal of Comparative Neurology, 527(1), pp.13-37.

Pessoa, D.M.A., Maia, R., de Albuquerque Ajuz, R.C., De Moraes, P.Z.P.M.R., Spyrides, M.H.C. and Pessoa, V.F., 2014. The adaptive value of primate color vision for predator detection. American journal of primatology, 76(8), pp.721-729.

Qiu, Y., Zhao, Z., Klindt, D., Kautzky, M., Szatko, K.P., Schaeffel, F., Rifai, K., Franke, K., Busse, L. and Euler, T., 2021. Natural environment statistics in the upper and lower visual field are reflected in mouse retinal specializations. Current Biology, 31(15), pp.3233-3247.

Rieke-Lab /calibration-resources. https://github.com/Rieke-Lab/calibration-resources /sources/mouse. Consulted in January 2025.

Rinner, O., Gegenfurtner, K.R., 2000. Time course of chromatic adaptation for color appearance and discrimination. Vision Research, 40(14), pp. 1813–1826.

Rosa, J.M., Morrie, R.D., Baertsch, H.C., Feller, M.B., 2016. Contributions of Rod and Cone Pathways to Retinal Direction Selectivity Through Development. Journal of Neuroscience, 36(37), pp. 9683–9695.

Stabio, M.E., Sabbah, S., Quattrochi, L.E., Ilardi, M.C., Fogerson, P.M., Leyrer, M.L., Kim, M.T., Kim, I., Schiel, M., Renna, J.M. and Briggman, K.L., 2018. The M5 cell: a color-opponent intrinsically photosensitive retinal ganglion cell. Neuron, 97(1), pp.150-163.

Stockman, A. and Sharpe, L.T., 2000. The spectral sensitivities of the middle-and long-wavelength-sensitive cones derived from measurements in observers of known genotype. *Vision research*, *40*(13), pp.1711-1737.

Szel, A., Röhlich, P., Gaffé, A.R., Juliusson, B., Aguirre, G.V. and Van Veen, T., 1992. Unique topographic separation of two spectral classes of cones in the mouse retina. Journal of Comparative Neurology, 325(3), pp.327-342.

Szatko, K.P., Korympidou, M.M., Ran, Y., Berens, P., Dalkara, D., Schubert, T., Euler, T. and Franke, K., 2020. Neural circuits in the mouse retina support color vision in the upper visual field. Nature communications, 11(1), p.3481.

Tikidji-Hamburyan, A., Reinhard, K., Storchi, R., Dietter, J., Seitter, H., Davis, K.E., Idrees, S., Mutter, M., Walmsley, L., Bedford, R.A., Ueffing, M., Ala-Laurila, P., Brown, T.M., Lucas, R.J., Münch, T.A., 2017. Rods progressively escape saturation to drive visual responses in daylight conditions. Nature Communnications, 8(1), p. 1813.

Tkačik, G., Garrigan, P., Ratliff, C., Milčinski, G., Klein, J.M., Seyfarth, L.H., Sterling, P., Brainard, D.H. and Balasubramanian, V., 2011. Natural images from the birthplace of the human eye. PLoS one, 6(6), p.e20409.

Turner, M.H., Schwartz, G.W. and Rieke, F., 2018. Receptive field center-surround interactions mediate context-dependent spatial contrast encoding in the retina. Elife, 7, p.e38841.

Valenta, K., Burke, R.J., Styler, S.A., Jackson, D.A., Melin, A.D. and Lehman, S.M., 2013. Colour and odour drive fruit selection and seed dispersal by mouse lemurs. Scientific reports, 3(1), p.2424.

Wang, J.-S., Kefalov, V.J., 2009. An Alternative Pathway Mediates the Mouse and Human Cone Visual Cycle. Current Biology, 19(19), pp. 1665–1669.

Wang, Y.V., Weick, M. and Demb, J.B., 2011. Spectral and temporal sensitivity of cone-mediated responses in mouse retinal ganglion cells. Journal of Neuroscience, 31(21), pp.7670-7681.

Yger, P., Spampinato, G.L., Esposito, E., Lefebvre, B., Deny, S., Gardella, C., Stimberg, M., Jetter, F., Zeck, G., Picaud, S. and Duebel, J., 2018. A spike sorting toolbox for up to thousands of electrodes validated with ground truth recordings in vitro and in vivo. eLife 7.

Yoshimatsu, T., Bartel, P., Schröder, C., Janiak, F.K., St-Pierre, F., Berens, P. and Baden, T., 2021. Ancestral circuits for vertebrate color vision emerge at the first retinal synapse. Science Advances, 7(42), p.eabj6815.

Yoshimatsu, T., Schröder, C., Nevala, N.E., Berens, P. and Baden, T., 2020. Fovea-like photoreceptor specializations underlie single UV cone driven prey-capture behavior in zebrafish. Neuron, 107(2), pp.320-337.

Yu, C., Wijntjes, M., Eisemann, E., Pont, S., 2023. Quantifying the spatial, temporal, angular and spectral structure of effective daylight in perceptually meaningful ways. Optics Express, 31(5), pp. 8953–8974.